

Electromagnetically driven convection suitable for mass transfer enhancement in liquid metal batteries

Weber, N.; Nimitz, M.; Personnettaz, P.; Salas, A.; Weier, T.;

Originally published:

July 2018

Applied Thermal Engineering 143(2018), 293-301

DOI: <https://doi.org/10.1016/j.applthermaleng.2018.07.067>

Perma-Link to Publication Repository of HZDR:

<https://www.hzdr.de/publications/Publ-26772>

Release of the secondary publication
on the basis of the German Copyright Law § 38 Section 4.

CC BY-NC-ND

Electromagnetically driven convection suitable for mass transfer enhancement in liquid metal batteries

Norbert Weber^a, Michael Nimitz^a, Paolo Personnettaz^{a,c}, Alejandro Salas^{a,b},
Tom Weier^a

^a*Helmholtz-Zentrum Dresden – Rossendorf, Bautzner Landstr. 400, Dresden, Germany*

^b*Instituto Tecnológico y de Estudios Superiores de Monterrey, Monterrey, Mexico*

^c*Politecnico di Torino, Corso Duca degli Abruzzi 24, 10129 Torino, Italy*

Abstract

Liquid metal batteries (LMBs) were recently proposed as cheap large scale energy storage. Such devices are urgently required for balancing highly fluctuating renewable energies. During discharge, LMBs tend to form intermetallic phases. These do not only limit the up-scalability, but also the efficiency of the cells. Generating a mild fluid flow in the fully liquid cell will smoothen concentration gradients and minimise the formation of intermetallics. In this context we study electro-vortex flow numerically. We simulate a recent LMB related experiment and discuss how the feeding lines to the cell can be optimised to enhance mass transfer. The Lorentz forces have to overcome the stable thermal stratification in the cathode of the cell; we show that thermal effects may reduce electro-vortex flow velocities considerable. Finally, we study the influence of the Earth magnetic field on the flow.

Keywords: liquid metal battery, mass transfer, electro-vortex flow, swirl, Rayleigh-Bénard convection, OpenFOAM

1. Introduction

Integrating highly fluctuating renewable energies (such as photovoltaics and wind power) into the electric grid calls for large scale energy storage. Such storage must be, first of all, safe and cheap. The liquid metal battery (LMB) promises both. After being intensively investigated in the 1960s, and abandoned later, LMB research experienced a renaissance some ten years ago. For an overview of the pioneering work, see [1–3] (recommended [4]) and for the recent work [5] and [6].

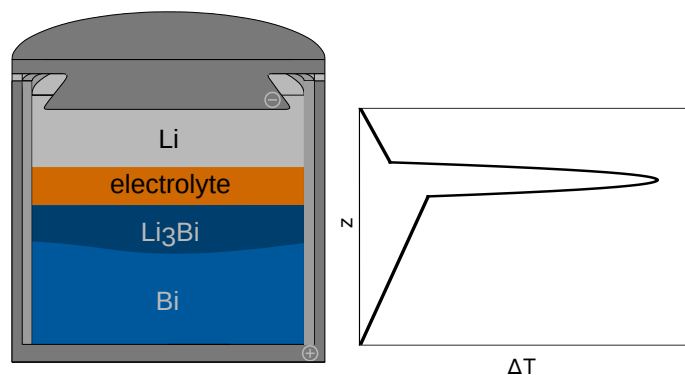


Figure 1: Sketch of a typical Li||Bi liquid metal battery with an intermetallic phase forming in the cathode (left) and vertical temperature distribution in the three layers for pure diffusion (right).

Fig. 1a shows a sketch of a typical LMB. A dense metal on the bottom (cathode, positive electrode) is separated by a liquid salt from a lighter metal at the top (anode, negative electrode). All three phases float above each other; the salt acts as the electrolyte. The word “liquid metal battery” names only a type of battery (which may consists of many different active metals). Typical cells include Ca||Bi [7, 8], Ca||Pb [9], K||Hg [10, 11], Li||Bi [1, 12–16], Li||Pb [1, 17], Li||Sb [5, 17], Li||Sn [1, 14, 18–20], Li||Zn [1], Mg||Sb [5, 21, 22], Na||Bi [1, 14, 18, 20, 23–27], Na||Hg [5, 28, 29], Na||Pb [1, 14, 20, 27, 30], Na||Sn [1, 11, 18, 20, 31, 32] and Na||Zn [33, 34] as well as exotic ones such as Li||Se [1, 35, 36] or Li||Te [1, 14, 15, 35, 36].

19 During discharge, the anode metal is oxidised, crosses the electrolyte layer
20 and alloys in the bottom layer with the dense metal (“concentration cell”).
21 Commonly, the ohmic resistance of the electrolyte layer represents the most im-
22 portant overvoltage. However, at higher discharge currents concentration polar-
23 isation enters the field [5, 11, 22, 28, 32, 37]. Example: when *discharging* a Li||Bi
24 cell, Li-rich alloy will concentrate at the cathode-electrolyte interface. When a
25 certain local concentration is exceeded, a solid intermetallic phase (Li_3Bi) will
26 form (fig. 1a) [1, 24]. Such intermetallics often float on the cathode metal [38].
27 Sometimes they expand during solidification. As the walls impede a lateral
28 expansion, the intermetallic will form a dome until finally short-circuiting the
29 electrolyte. Especially in Ca based cells, locally growing dendrites may addi-
30 tionally short-circuit the cell [7]. Besides of all the mentioned drawbacks, the
31 formation of intermetallics has one advantage: it removes anode metal from the
32 melt and keeps thereby the voltage constant. It should be also mentioned that
33 some intermetallics have high resistances while others are good conductors.

34 When *charging* the cell of fig. 1a, the cathode-electrolyte interface will de-
35plete of Li and a similar concentration gradient may develop [24]. This effect is
36undesirable, too. Finally, all the same effects may theoretically happen in the
37anode compartment, too, if an alloyed top electrode is used (e.g. CaMg [8, 21]).
38However, such effects were not reported, yet.

39 It was early proposed that a mild fluid flow may counterbalance concentra-
40tion gradients and increase thereby the efficiency of LMBs [1, 24, 37]. While
41“mechanical stirring” [1, 37] seems difficult to realise, a localised heating or cool-
42ing inducing thermal convection may be a very good option [39, 40]. Electro-
43vortex flow (EVF) may be used for an efficient mass transfer enhancement, too
44[41–43]. Simply saying, EVF always may develop when current lines are not in
45parallel. It can therefore easily be adjusted by choosing the diameter/geometry
46of the current collectors and feeding lines appropriately. EVF drives a jet away
47from the wall, forming a poloidal flow [44]. For a classical example of the origin
48of EVF, see Lundquist [44] and Shercliff [45], for a good introduction David-
49son [46] and a detailed overview including many experiments Bojarevics et al.

50 [47]. Its relevance for LMBs is outlined by Ashour et al. [43]. It should also
 51 be mentioned that other flow phenomena like the Taylor instability [48–56] ,
 52 Rayleigh-Bénard convection [57, 58] or interface instabilities [59–63] may en-
 53 hance mass transfer in LMBs, as well.

54 This article is dedicated (mainly) to electro-vortex flow. It’s aim is twofold:
 55 first, we will show how the connection of the supply lines to the cell influences the
 56 flow. Second, we study how electro-vortex flow and thermal convection interact.
 57 For this purpose we combine numerical simulation with a simple 1D conduction
 58 model. These models – and the experiment which inspired our studies – are
 59 described in the following section.

60 2. Physical, mathematical and numerical model

61 In this section we will first present the experiment [64] which inspired this
 62 article. Thereafter we explain the way in which we estimate the temperature
 63 gradient appearing in the cathode of a liquid metal battery (LMB). Finally, we
 64 give an introduction to the 3D numerical models used.

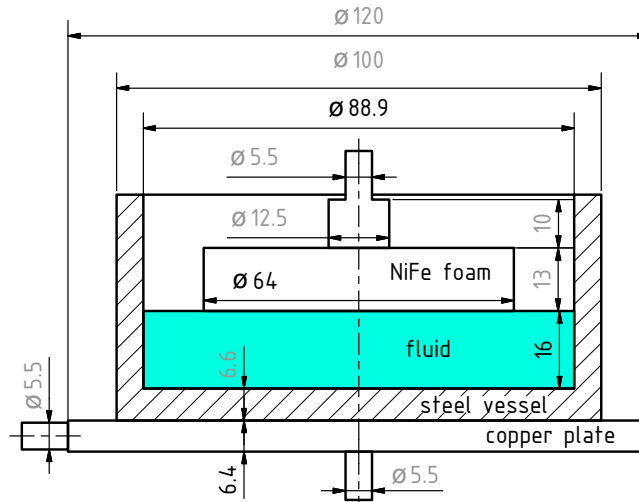


Figure 2: Dimensions of the experiment and simulation model (in mm). The grey values are not exactly known; they are estimated from the sketch in [64]. The wires are assumed to be made of copper.

65 Fig. 2 illustrates the mentioned experiment, conducted by Kelley & Sadoway
 66 [64]. A cylindrical steel vessel contains a melt of eutectic lead-bismuth at 150 °C.
 67 An electric current (up to 0.375 A/cm²) is applied between a bottom and top
 68 electrode. The bottom electrode may be attached centrally or laterally. The
 69 upper electrode consists of a nickel-iron foam; such foam is often used in LMBs
 70 to contain the anode metal [6]. As the setup is heated from below, Rayleigh-
 71 Bénard cells appear. If an internal current is applied, the flow becomes much
 72 more regular at 0.05 A/cm². It is deduced that convection cells align with the
 73 magnetic field. It is further claimed that the copper plate which placed between
 74 the bottom electrode and the the vessel, “ensures a uniform current density” in
 75 the melt. We will show that this is not exactly true; we will further demonstrate
 76 how electro-vortex flow may give an alternative explanation for the increase in
 77 order.

78 We use the following material properties of eutectic PbBi at 150 °C [43]:
 79 a kinematic viscosity of $\nu = 2.7 \cdot 10^{-7} \text{ m}^2/\text{s}$, a thermal expansion coefficient
 80 of $\beta = 1.3 \cdot 10^{-4} \text{ K}^{-1}$, an electric conductivity of $\sigma = 9 \cdot 10^5 \text{ S/m}$, a density
 81 of $\rho = 10\,505 \text{ kg/m}^3$, an isobaric heat capacity of $c_p = 148 \text{ J/kg/K}$, a heat
 82 conductivity of $\lambda = 10 \text{ W/m/K}$, a thermal diffusivity of $\alpha = 6 \cdot 10^{-6} \text{ m}^2/\text{s}$, a
 83 Prandtl number of $Pr = 0.04$ and a sound velocity of $u_s = 1\,765 \text{ m/s}$ [65–67].
 84 The electric conductivity of the vessel is assumed to be $\sigma = 1.37 \cdot 10^6 \text{ S/m}$ and
 85 of the wires and copper plate $\sigma = 58.1 \cdot 10^7 \text{ S/m}$. The electric conductivity of
 86 the Fe-Ni foam is not easy to determine; we use a value of $\sigma = 1.37 \cdot 10^6 \text{ S/m}$
 87 without further justification.

88 Geometrically, the described experiment perfectly represents a liquid cath-
 89 ode of an LMB. However, the temperature gradient in a working LMB depends
 90 on the boundary conditions. For a single cell in an environment at room tem-
 91 perature it will rather be opposite to that in the experiment. As the electrolyte
 92 layer has the highest resistance (four orders larger than the metals), most heat
 93 will be generated there [57]. Fig. 1b shows a typical vertical temperature profile
 94 through all three layers. If no thermal management system induces additional
 95 temperature gradients (as suggested in [21, 40]) a stable thermal stratification

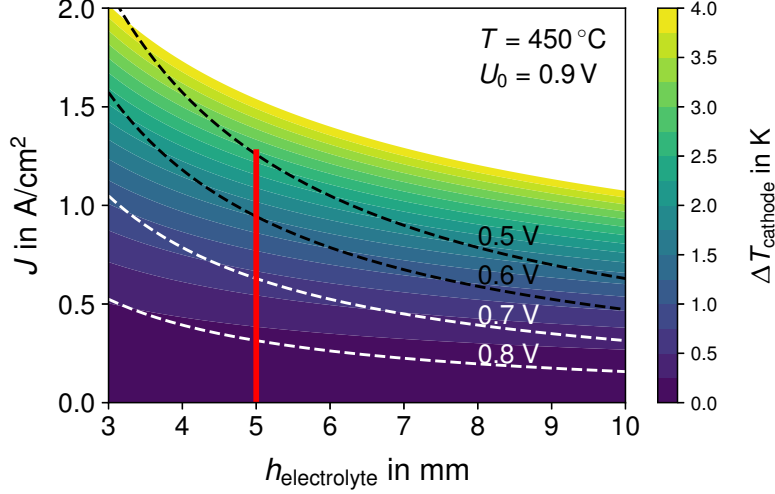


Figure 3: Temperature difference in the cathode for pure conduction in a Li||Bi cell. The same model and material properties as in [68] are used.

96 is expected in the cathode. To drive a flow there, any force has to overcome
 97 first this stable stratification.

98 The temperature difference between top and bottom of the cathode can be
 99 estimated using the simple 1D heat conduction model developed by Personnettaz
 100 et al. [68] (for a 3D study of heat transfer in a Li||PbBi cell, see [69]). He
 101 considers a Li|LiCl-KCl|Bi cell operating at 450°C. Although our cathode is
 102 made of eutectic PbBi (and not Bi), we use the same model to get a rough
 103 *estimate* of the temperature gradient in the cathode. The Li-layer is assumed
 104 to be 32 and the Bi-layer 16 mm thick; for the material parameters, see [68].
 105 Depending on the current density and thickness of the electrolyte, the ΔT over
 106 the cathode changes as illustrated in fig. 3. In our numerical simulation we will
 107 assume the electrolyte to be 5 mm thick (realistic values are 3-15 mm [70]). We
 108 will use the temperature difference of fig. 3 as boundary condition as

$$\Delta T = \frac{h_{\text{Bi}} h_{\text{salt}} q (2h_{\text{Li}} \lambda_{\text{salt}} + h_{\text{salt}} \lambda_{\text{Li}})}{2h_{\text{Bi}} \lambda_{\text{Li}} \lambda_{\text{salt}} + 2h_{\text{Li}} \lambda_{\text{Bi}} \lambda_{\text{salt}} + 2h_{\text{salt}} \lambda_{\text{Bi}} \lambda_{\text{Li}}}, \quad (1)$$

109 with h , λ and q denoting the layer heights, the thermal conductivities and the

110 volumetric heat source in the electrolyte. We will study, if electro-vortex flow
 111 can overcome the stable stratification.

112 The numerical model is implemented in OpenFOAM [71]; the electro-vortex
 113 flow solver is explained in detail in [72]. Basically, it computes the electric
 114 potential ϕ and current density \mathbf{J} on a global mesh as

$$\nabla \cdot \sigma \nabla \phi = 0 \quad (2)$$

$$\mathbf{J} = -\sigma \nabla \phi \quad (3)$$

115 with σ denoting the electric conductivity. All conducting regions (of different
 116 conductivities) are fully coupled. The results are then mapped on a separate
 117 fluid mesh. Induced currents and magnetic fields are neglected, which is justified
 118 as long as the velocities are small. On the fluid mesh the following set of
 119 equations is solved:

$$\frac{\partial \mathbf{u}}{\partial t} + (\mathbf{u} \cdot \nabla) \mathbf{u} = -\nabla p + \nu \Delta \mathbf{u} + \frac{\mathbf{J} \times \mathbf{B}}{\rho} \quad (4)$$

$$\mathbf{B}(\mathbf{r}) = \frac{\mu_0}{4\pi} \int \frac{\mathbf{J}(\mathbf{r}') \times (\mathbf{r} - \mathbf{r}')}{|\mathbf{r} - \mathbf{r}'|^3} dV' \quad (5)$$

$$0 = \Delta \mathbf{B} \quad (6)$$

120 with t , \mathbf{u} , p , ν , ρ , μ_0 , \mathbf{r} and V denoting the time, the velocity, the pressure, the
 121 kinematic viscosity, the density, the vacuum permeability, the coordinate and
 122 the cell volume, respectively. The Biot-Savart integral is only used to determine
 123 the magnetic field \mathbf{B} on the boundaries. The fluid mesh has at least 200 cells
 124 on the diameter, which is fine enough according to [43].

125 If thermal effects shall be included, the Oberbeck-Boussinesq approximation
 126 [73] is used (for its validity, see [43, 74]). The following set of equations is solved

$$\frac{\partial \mathbf{u}}{\partial t} + \nabla \cdot (\mathbf{u}\mathbf{u}) = -\nabla p_d + \nu \Delta \mathbf{u} - \mathbf{g} \cdot \mathbf{r} \nabla \rho_k + \frac{\mathbf{J} \times \mathbf{B}}{\rho_0} \quad (7)$$

$$\nabla \cdot \mathbf{u} = 0 \quad (8)$$

$$\frac{\partial T}{\partial t} + \nabla \cdot (\mathbf{u}T) = \frac{\lambda}{\rho_0 c_p} \Delta T \quad (9)$$

127 with \mathbf{u} , p , ν , \mathbf{g} , \mathbf{r} , T , c_p , \mathbf{J} and σ denoting velocity, pressure, kinematic viscosity,
 128 gravity, position vector, temperature, specific heat capacity, current density and

129 electric conductivity, respectively. The density $\rho = \rho_0 \rho_k = \rho_0(1 - \beta(T - T_{\text{ref}}))$
 130 is calculated using the mean density ρ_0 at reference temperature T_{ref} and the
 131 coefficient of thermal expansion β ; \mathbf{J} and \mathbf{B} are determined by the electro-vortex
 132 solver as described above. At least 250 cells on the diameter and strongly refined
 133 boundary layers are used.

134 3. Results

135 This section is arranged as follows: firstly, we compare the influence of a
 136 symmetric and asymmetric current supply on pure electro-vortex flow (fig. 4).
 137 Thereafter, we study the influence of the Earth magnetic field and of thermal
 138 stratification on both connection types (fig. 5 and 6). Further, we give estimates
 of the flow velocity depending on the cell current.

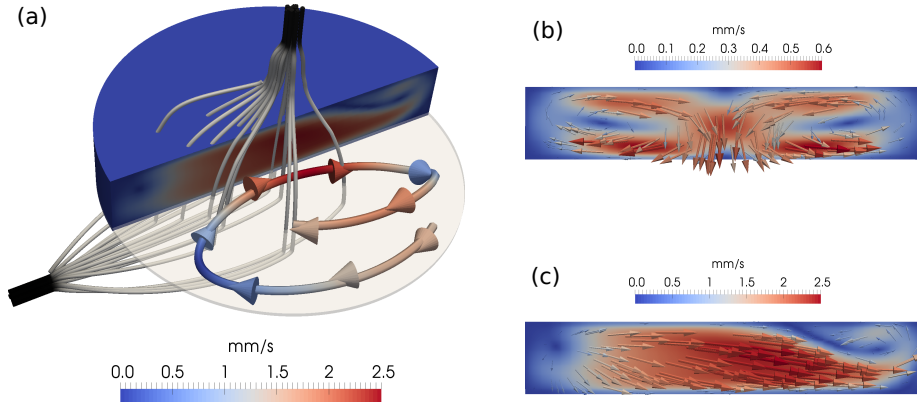


Figure 4: Current path and velocity streamlines for a current supply from the side (a). Velocity
 on a vertical plane for symmetric (b) and lateral current supply (c). The current is $I = 40$ A;
 the results show electro-vortex flow alone.

139
 140 Fig. 4a illustrates the current path, streamlines and velocities for a lateral
 141 supply line. Electro-vortex flow is simulated alone; the applied current is 40 A.
 142 The flow profile is essentially horizontal forming two kidney-shaped vortices.
 143 The velocity reaches 2.5 mm/s. The *horizontal* jet (also shown in 4c) is uncom-
 144 mon for electro-vortex flow, but can easily be explained. As the current flows
 145 mainly horizontally through the copper plate, it induces a magnetic field in the

146 fluid. This field points towards the observer (in fig. 4a and c). The current in
 147 the liquid metal flows upwards (vertically) and interacts with the induced field.
 148 Consequently, the Lorentz force points to the right and drives the observed flow
 149 in “prolongation” of the current supply. For similar experiments, see [75, 76].

150 Fig. 4b shows the flow profile for a symmetric current supply, again for 40 A.
 151 A typical poloidal flow develops as it was often observed experimentally [47, 77–
 152 81]. Similar flow structures are very well known from vacuum arc remelting and
 153 electro-slag remelting [82–89]. However, depending on the exact geometry, the
 154 direction of the flow might be reversed [90–93]. In our simulation, the velocities
 155 reach 0.6 mm/s for the symmetrical setup. This is only 25 % of the flow velocity
 156 observed for a lateral current supply. Due to the shallow liquid metal layer, a
 157 poloidal flow will dissipate strongly in the boundary layer.

158 The simulated velocities are not directly comparable to the experiment. The
 159 latter was additionally heated from below (vertical temperature difference of ap-
 160 proximately $\Delta T = 10$ K). As shown numerically by Beltrán, the experimentally
 161 observed flow is mainly caused by Rayleigh-Bénard convection. Also he used a
 162 volumetric expansion coefficient three times smaller than the real one [64, 94]
 163 (for the correct value see [43]), his velocity profile and magnitude (3 mm/s)
 164 matches very well to the experimental results (compare fig. 9 in [94] and fig. 4
 165 in [64]). Electro-vortex flow will generally lead to velocities one order of mag-
 166 nitude smaller (Kelley and Sadoway [64] used currents of 23.3 A at most; our
 167 results are for 40 A). However, electro-vortex flow will surely influence the flow
 168 structure and may explain the increase in order of the flow which was observed
 169 experimentally.

170 In the next step we focus on the symmetric current supply (with the poloidal
 171 flow) only, and analyse the influence of a vertical magnetic background field.
 172 When we add the magnetic field of the Earth (measured in Dresden as $\mathbf{B} =$
 173 $(15 \cdot \mathbf{e}_x, 5 \cdot \mathbf{e}_y, 36 \cdot \mathbf{e}_z) \mu\text{T}$) the original poloidal flow (fig. 5a) becomes strongly
 174 helical (fig. 5b). The appearance of such azimuthal swirl flow is well known from
 175 experiments [43, 77, 95] and can be easily explained. Radial cell currents and a
 176 vertical magnetic background field lead to azimuthal Lorentz forces [79, 84, 95].

177 Compared to a recent experiment by Ashour [43] with a point electrode on the
178 top, we observe considerably stronger swirl (compare fig. 5b with fig. 5 in [43]).
179 We attribute this difference to the location of the azimuthal forcing. Here, the
180 force is well distributed in the whole volume; in [43] it is concentrated only in
181 the centre of the liquid metal “sheet”. We suppose the distributed azimuthal
182 Lorentz force to better suppress the poloidal flow by forcing the streamlines into
183 a dissipative Ekman layer [84]. Fig. 5c shows the volume averaged mean velocity
184 of the poloidal and azimuthal flow – with and without the Earth magnetic field.
185 If we add a vertical field, azimuthal swirl appears (compare the dashed curve).
186 At the same time, the poloidal flow is strongly reduced (by a factor of 1/2). This
187 fits nicely to Davidsons “poloidal suppression” model [84]. This is remarkable,
188 because simulations with a point electrode (see [43]) did not show such a strong
189 suppression.

190 Keeping the symmetric current supply, we now focus on the influence of the
191 temperature stratification. During operation of an LMB, the cathode will be
192 heated from above; the temperature stratification will be stable. At first glance,
193 this configuration is similar to arc remelting. There, an electric arc heats the
194 melt from above. However, the bath is cooled rather from the side than from
195 below which leads to strong thermally driven flow [96], but we have a stable
196 thermal stratification instead. Based on the temperature conduction model
197 described in section 2 we apply a vertical temperature gradient of $\Delta T = 0.7$ K
198 (at 40 A). The stable thermal stratification slows down the electro-vortex flow
199 (compare fig. 5d and e). While the general flow structure does not change,
200 especially the velocity near the bottom wall decreases by a factor of 2/3. This
201 result cannot be compared to the experiment, as Kelley and Sadoway heated
202 from below (and we from above). A temperature gradient as in the experiment
203 is not expected to appear during “normal” operation of an LMB; however, an
204 additional heating or cooling for mass transfer enhancement (as proposed in
205 [39, 40]) can easily lead to similar configurations.

206 We use two quantities to estimate the mass transfer in the cathode: the
207 volume averaged velocity as global measure, and the mean velocity gradient at

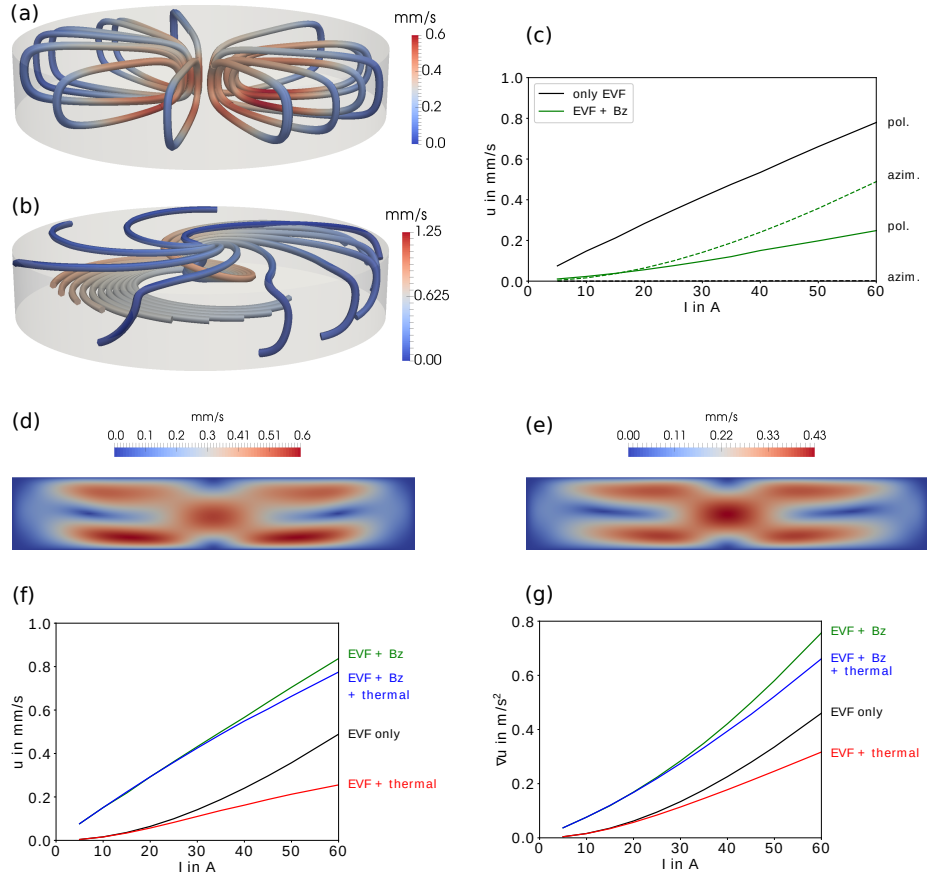


Figure 5: Streamlines and velocity without (a) and with the Earth magnetic field (b). Volume averaged mean velocities of the azimuthal and poloidal flow for both cases (c). Velocity on a vertical plane for symmetric current supply without temperature (d) and with a negative temperature gradient of 0.7K (e). Volume averaged mean velocity (f) and mean velocity gradient (g) of electro-vortex flow alone, with an additional Earth magnetic field (Bz) and with a stabilising temperature gradient. $I = 40$ A.

208 the foam-cathode interface as local one. Fig. 5f and g show both quantities
 209 for electro-vortex flow alone, with the Earth magnetic field (“Bz”) and with a
 210 stabilising thermal gradient. The azimuthal flow, caused by the Earth magnetic
 211 field, yields the highest velocities. A vertical temperature gradient does barely
 212 influence the horizontal flow. The poloidal electro-vortex flow (“EVF alone”) is
 213 considerably slower – it is strongly dissipated at the bottom wall. The vertical

214 temperature gradient effectively breaks the downwards flow. Interestingly, a
215 strong flow in the volume leads also to strong velocity gradients at the interface.

216 We now consider the lateral current supply, and study again the influence
217 of temperature and the Earth magnetic field. The prevailing horizontal flow is
218 hardly influenced by a stabilising vertical temperature gradient. The flow struc-
219 ture changes only slightly; the velocities with and without temperature gradient
220 are almost the same (compare fig. 6c and d). Taking into account the Earth
221 magnetic field changes the flow much more (compare fig. 6a and b). The hori-
222 zontal current and vertical magnetic background field generate a Lorentz force
223 which deflects the jet in clockwise direction. Presumably the stronger dissipa-
224 tion in the boundary layers decreases the velocity slightly. Most importantly,
225 the Earth magnetic field does not lead to swirl flow in this configuration – the
226 jet is only deflected. Fig. 6e and f show the mean velocity and the mean velocity
227 gradient for pure electro-vortex flow, with the Earth magnetic field and with
228 the stabilising temperature gradient. The differences are only marginal.

229 4. Summary & outlook

230 We have discussed, how electro-vortex flow (EVF) has the potential to en-
231 hance mass transfer in liquid metal batteries (LMBs). In a first step we discussed
232 why such mass transfer enhancement is important. We emphasised that mostly
233 (but not only) mixing of the cathode during discharge is highly beneficial. We
234 studied the flow structure and magnitude of EVF numerically. Moreover, we
235 discussed the influence of stray magnetic fields, the connection of the supply
236 lines and a stable thermal stratification on electro-vortex flow.

237 A lateral current supply to the cathode will generate a *horizontal* flow. In
238 contrast, a central current supply below the cathode will induce a *vertical* jet.
239 Looking only on this flow-direction, would expect a vertical flow to be bet-
240 ter suited for enhancing mass transfer. It will remove reaction products di-
241 rectly from the cathode-electrolyte interface. However, the vertical (or better:
242 poloidal) flow has three disadvantages: (1) it's mean velocity is much smaller

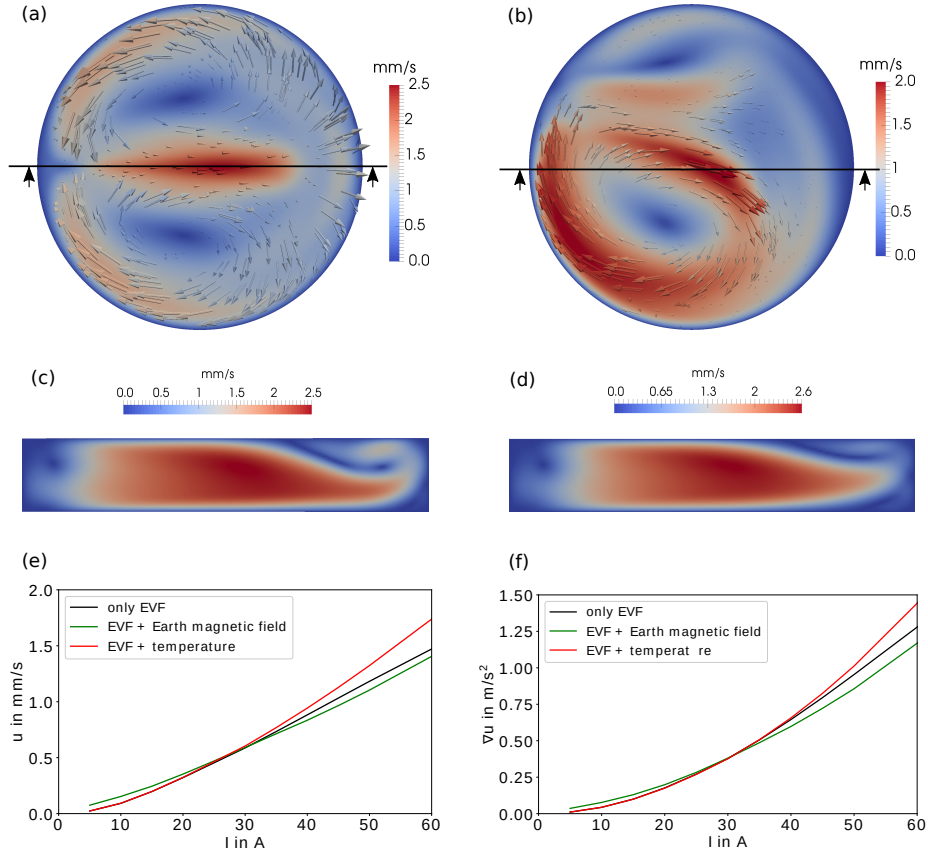


Figure 6: Electro-vortex flow for a lateral supply wire without (a) and with the Earth magnetic field (b). Flow in the cross section of the jet without (c) and with a stabilising thermal gradient (d). The current for (a)-(d) is 40 A. Volume averaged mean velocity (e) and mean velocity gradient (f) for electro-vortex flow alone, with the additional Earth magnetic field (B_z) and with a stabilising temperature gradient.

243 compared to the horizontal flow, (2) it is dampened by the stable temperature
 244 stratification and (3) it will turn to a swirling flow under presence of the Earth
 245 magnetic field. In contrast, the horizontal jet will not be dampened considerably
 246 by a temperature stratification nor be strongly influenced by the Earth mag-
 247 netic field. We believe therefore the lateral supply line to be better suited for
 248 enhancing mass transfer. Concerning the swirl flow we could (at least partially)
 249 confirm Davidsons model of poloidal suppression.

250 Our models are strongly simplified: we ignore induced currents and mag-
251 netic fields; we ignore internal heating; the simulation of thermal convection
252 and EVF is fully decoupled. A next step would be therefore the development
253 of a fully coupled EVF-thermal convection model as well as it's coupling with a
254 real mass transfer (e.g. Li in Bi) model. Of course, velocity and concentration
255 measurements in a real 3-layer LMB would be a large step forward. Performing
256 Kelley's experiment with an inverse temperature gradient (better at room tem-
257 perature) could allow a further experimental study of the interaction between
258 EVF and thermal convection.

259 **Acknowledgements**

260 This work was supported by the Deutsche Forschungsgemeinschaft (DFG,
261 German Research Foundation) by award number 338560565 as well as the
262 Helmholtz-Gemeinschaft Deutscher Forschungszentren (HGF) in frame of the
263 Helmholtz Alliance "Liquid metal technologies" (LIMTECH). The computa-
264 tions were performed on the Bull HPC-Cluster "Taurus" at the Centre for In-
265 formation Services and High Performance Computing (ZIH) at TU Dresden and
266 on the cluster "Hydra" at Helmholtz-Zentrum Dresden – Rossendorf. Fruitful
267 discussions with V. Bojarevics, P. Davidson, D. Kelley, F. Stefani and T. Vogt
268 on several aspects of electro-vortex flow and thermal convection are gratefully
269 acknowledged. N. Weber thanks Henrik Schulz for the HPC support.

270 **References**

- 271 [1] E. J. Cairns, C. E. Crouthamel, A. K. Fischer, M. S. Foster, J. C. Hesson,
272 C. E. Johnson, H. Shimotake, A. D. Tevebaugh, Galvanic Cells with Fused-
273 Salt Electrolytes, ANL-7316, Argonne National Laboratory, 1967.
- 274 [2] H. L. Chum, R. A. Osteryoung, Review of Thermally Regenerative Elec-
275 trochemical Systems, Solar Energy Research Institute, 1980.

- 276 [3] H. L. Chum, R. A. Osteryoung, Review of Thermally Regenerative Elec-
277 trochemical Cells, Solar Energy Research Institute, 1981.
- 278 [4] D. A. J. Swinkels, Molten Salt Batteries and Fuel Cells, in: J. Braunstein,
279 G. Mamantov, G. P. Smith (Eds.), Advances in Molten Salt Chemistry,
280 Vol. 1, Plenum Press, New York, 1971, pp. 165–223.
- 281 [5] H. Kim, D. A. Boysen, J. M. Newhouse, B. L. Spatocco, B. Chung, P. J.
282 Burke, D. J. Bradwell, K. Jiang, A. A. Tomaszowska, K. Wang, W. Wei,
283 L. A. Ortiz, S. A. Barriga, S. M. Poizeau, D. R. Sadoway, Liquid Metal
284 Batteries: Past, Present, and Future, Chem. Rev. 113 (3) (2013) 2075–2099.
285 doi:10.1021/cr300205k.
- 286 [6] D. H. Kelley, T. Weier, Fluid mechanics of liquid metal batteries, Appl.
287 Mech. Rev. doi:10.1115/1.4038699.
- 288 [7] H. Kim, D. A. Boysen, T. Ouchi, D. R. Sadoway, Calcium - bismuth elec-
289 trodes for large - scale energy storage, J. Power Sources 241 (2013) 239–248.
- 290 [8] T. Ouchi, H. Kim, B. L. Spatocco, D. R. Sadoway, Calcium-based multi-
291 element chemistry for grid-scale electrochemical energy storage, Nat. Com-
292 mun. 7 (2016) 10999. doi:10.1038/ncomms10999.
- 293 [9] S. Poizeau, H. Kim, J. M. Newhouse, B. L. Spatocco, D. R. Sadoway,
294 Determination and modeling of the thermodynamic properties of liquid
295 calcium–antimony alloys, Electrochimica Acta 76 (2012) 8–15. doi:10.
296 1016/j.electacta.2012.04.139.
- 297 [10] B. Agruss, H. R. Karas, First Quarterly Technical Progress Report on
298 Design and Development of a Liquid Metal Cell for the Period 1 January
299 1962 – 31 March 1962, Tech. Rep. AD 274 197, Armed Service Technical
300 Information Agency (1962).
- 301 [11] B. Agruss, H. R. Karas, The Thermally Regenerative Liquid Metal Con-
302 centration Cell, in: R. F. Gold (Ed.), Regenerative EMF Cells, Vol. 64

- 303 of Advances in Chemistry, American Chemical Society, Washington, D.C.,
304 1967, pp. 62–81.
- 305 [12] S. Lawroski, R. C. Vogel, M. Levenson, V. H. Munnecke, Chemical engi-
306 neering summary report, Tech. Rep. ANL-6648, Argonne National Labo-
307 ratory (1963).
- 308 [13] M. S. Foster, S. E. Wood, C. E. Crouthamel, Thermodynamics of Binary
309 Alloys. I. The Lithium-Bismuth System, *Inorg. Chem.* 3 (10) (1964) 1428–
310 1431.
- 311 [14] R. C. Vogel, M. Levenson, J. H. Schraidt, J. Royal, Chemical engineer-
312 ing division research highlights, Tech. Rep. ANL-7175, Argonne National
313 Laboratory (1966).
- 314 [15] H. Shimotake, G. L. Rogers, E. J. Cairns, Secondary Cells with Lithium
315 Anodes and Immobilized Fused-Salt Electrolytes, *Ind. Eng. Chem. Process*
316 *Des. Dev.* 8 (1) (1969) 51–56.
- 317 [16] X. Ning, S. Phadke, B. Chung, H. Yin, P. Burke, D. R. Sadoway, Self-
318 healing Li–Bi liquid metal battery for grid-scale energy storage, *J. Power*
319 *Sources* 275 (2015) 370–376. doi:10.1016/j.jpowsour.2014.10.173.
- 320 [17] K. Wang, K. Jiang, B. Chung, T. Ouchi, P. J. Burke, D. A. Boysen, D. J.
321 Bradwell, H. Kim, U. Muecke, D. R. Sadoway, Lithium–antimony–lead
322 liquid metal battery for grid-level energy storage, *Nature* 514 (7522) (2014)
323 348–350. doi:10.1038/nature13700.
- 324 [18] R. C. Vogel, M. Levenson, F. R. Masten, Chemical engineering division
325 research highlights, Tech. Rep. ANL-7020, Argonne National Laboratory
326 (1965).
- 327 [19] M. S. Foster, C. E. Crouthamel, S. E. Wood, Thermodynamics of Binary
328 Alloys. II. The Lithium-Tin System, *J. Phys. Chem.* 70 (10) (1966) 3042 –
329 3045.

- 330 [20] J. C. Hesson, H. Shimotake, Thermodynamics and thermal efficiencies of
331 thermally regenerative bimetallic and hydride emf cell systems, in: Regen-
332 erative EMF Cells, American Chemical Society, 1967, pp. 82–104.
- 333 [21] D. J. Bradwell, Liquid Metal Batteries: Ambipolar Electrolysis and Alka-
334 line Earth Electroalloying Cells, Ph.D. thesis, Massachusetts Institute of
335 Technology (2011).
- 336 [22] D. J. Bradwell, H. Kim, A. H. C. Sirk, D. R. Sadoway, Magnesium–Antimony Liquid Metal Battery for Stationary Energy Storage, *J.*
337 *Am. Chem. Soc.* 134 (4) (2012) 1895–1897. doi:10.1021/ja209759s.
- 339 [23] M. S. Foster, G. H. McCloud, E. J. Cairns, Electrochemical studies of the
340 Sodium-Bismuth system, *J. Am. Chem. Soc.* (1967) 276–281.
- 341 [24] R. C. Vogel, M. Levenson, E. R. Proud, J. Royal, Chemical engineering
342 division research highlights, Tech. Rep. ANL-7350, Argonne National Lab-
343 oratory (1967).
- 344 [25] R. C. Vogel, M. Levenson, F. R. Masten, Chemical engineering division
345 semiannual report, Tech. Rep. ANL-7055, Argonne National Laboratory
346 (1965).
- 347 [26] H. Shimotake, E. J. Cairns, Bimetallic galvanic cells with fused-salt elec-
348 trolytes, in: *Advances in Energy Conversion Engineering*, ASME, Florida,
349 1967, pp. 951–962.
- 350 [27] R. C. Vogel, M. Levenson, J. H. Schraidt, J. Royal, Chemical engineering
351 semiannual report, Tech. Rep. ANL-7225, Argonne National Laboratory
352 (1966).
- 353 [28] L. A. Herédy, M. L. Iverson, G. D. Ulrich, H. L. Recht, Development of
354 a thermally regenerative Sodium-Mercury galvanic system Part I Electro-
355 chemical and Chemical Behavior of Sodium-Mercury Galvanic Cells, in:
356 *Regenerative EMF Cells*, American Chemical Society, 1967, pp. 30–42.

- 357 [29] B. L. Spatocco, P. J. Burke, D. R. Sadoway, Low temperature liquid metal
358 batteries for grid-scaled storage, 0099522 A1 (2014).
- 359 [30] A. Kiswa, J. Kazmierczak, B. Borresen, G. M. Haarberg, R. Tunold, The
360 Kinetics of the Sodium Electrode Reaction in Molten Sodium Chloride, *J.*
361 *Electrochem. Soc.* 142 (4) (1995) 1035–1040.
- 362 [31] R. D. Weaver, S. W. Smith, N. L. Willmann, The Sodium-Tin Liquid-Metal
363 Cell, *J. Electrochem. Soc.* 109 (8) (1962) 653–657.
- 364 [32] B. Agruss, The Thermally Regenerative Liquid-Metal Cell, *J. Electrochem.*
365 *Soc.* 110 (11) (1963) 1097–1103.
- 366 [33] J. Xu, O. S. Kjos, K. S. Osen, A. M. Martinez, O. E. Kongstein, G. M.
367 Haarberg, Na-Zn liquid metal battery, *J. Power Sources* 332 (2016) 274–
368 280. doi:10.1016/j.jpowsour.2016.09.125.
- 369 [34] J. Xu, A. M. Martinez, K. S. Osen, O. S. Kjos, O. E. Kongstein, G. M.
370 Haarberg, Electrode Behaviors of Na-Zn Liquid Metal Battery, *J. Elec-*
371 *trochem. Soc.* 164 (12) (2017) A2335–A2340.
- 372 [35] E. J. Cairns, H. Shimotake, High-Temperature Batteries, *Science* 164
373 (1969) 1347–1355.
- 374 [36] E. J. Cairns, H. Shimotake, Recent advances in fuel cells and their appli-
375 cation to new hybrid systems, *Adv. Chem.* 90 (1969) 321–350.
- 376 [37] M. S. Foster, Laboratory Studies of Intermetallic Cells, in: *Regenerative*
377 *EMF Cells*, American Chemical Society, 1967, pp. 136–148.
- 378 [38] T. Ouchi, H. Kim, X. Ning, D. R. Sadoway, Calcium-Antimony Alloys as
379 Electrodes for Liquid Metal Batteries, *J. Electrochem. Soc.* 161 (12) (2014)
380 A1898–A1904.
- 381 [39] D. Bradwell, G. Ceder, L. A. Ortiz, D. R. Sadoway, Liquid electrode bat-
382 tery, US patent 2011/0014505 A1 (2011).

- 383 [40] D. Bradwell, G. Ceder, L. A. Ortiz, D. R. Sadoway, Liquid metal alloy
384 energy storage device, US patent 9,076,996 B2 (2015).
- 385 [41] N. Weber, V. Galindo, J. Priede, F. Stefani, T. Weier, The influence of
386 current collectors on Tayler instability and electro vortex flows in liquid
387 metal batteries, *Phys. Fluids* 27 (014103).
- 388 [42] F. Stefani, V. Galindo, C. Kasprzyk, S. Landgraf, M. Seilmayer, M. Starace,
389 N. Weber, T. Weier, Magnetohydrodynamic effects in liquid metal batter-
390 ies, *IOP Conf. Ser. Mater. Sci. Eng.* 143 (2016) 012024. doi:10.1088/
391 1757-899X/143/1/012024.
- 392 [43] R. Ashour, D. H. Kelley, A. Salas, M. Starace, N. Weber, T. Weier, Com-
393 peting forces in liquid metal electrodes and batteries, *J. Power Sources* 378
394 (2018) 301–310. doi:10.1016/j.jpowsour.2017.12.042.
- 395 [44] S. Lundquist, On the hydromagnetic viscous flow generated by a diverging
396 electric current, *Ark. För Fys.* 40 (5) (1969) 89–95.
- 397 [45] J. A. Shercliff, Fluid motions due to an electric current source, *J. Fluid*
398 *Mech.* 40 (1970) 241–250.
- 399 [46] P. A. Davidson, *An Introduction to Magnetohydrodynamics*, Cambridge
400 *texts in applied mathematics*, Cambridge University Press, Cambridge ;
401 New York, 2001.
- 402 [47] V. Bojarevičs, Y. Freibergs, E. I. Shilova, E. V. Shcherbinin, *Electrically*
403 *Induced Vortical Flows*, Kluwer Academic Publishers, 1989.
- 404 [48] Y. V. Vandakurov, Theory for the stability of a star with a toroidal mag-
405 netic field, *Astron Zh* 49 (2) (1972) 324–333.
- 406 [49] F. Stefani, T. Weier, T. Gundrum, G. Gerbeth, How to circumvent the size
407 limitation of liquid metal batteries due to the Tayler instability, *Energy*
408 *Convers. Manag.* 52 (2011) 2982–2986.

- 409 [50] M. Seilmayer, F. Stefani, T. Gundrum, T. Weier, G. Gerbeth, M. Gellert,
410 G. Rüdiger, Experimental Evidence for a Transient Tayler Instability in a
411 Cylindrical Liquid-Metal Column, *Phys. Rev. Lett.* 108 (244501).
- 412 [51] N. Weber, V. Galindo, F. Stefani, T. Weier, T. Wondrak, Numerical simu-
413 lation of the Tayler instability in liquid metals, *New J. Phys.* 15 (043034).
- 414 [52] N. Weber, V. Galindo, F. Stefani, T. Weier, Current-driven flow instabili-
415 ties in large-scale liquid metal batteries, and how to tame them, *J. Power*
416 *Sources* 265 (2014) 166–173. doi:10.1016/j.jpowsour.2014.03.055.
- 417 [53] N. Weber, V. Galindo, F. Stefani, T. Weier, The Tayler instability at low
418 magnetic Prandtl numbers: Between chiral symmetry breaking and he-
419 licity oscillations, *New J. Phys.* 17 (11) (2015) 113013. doi:10.1088/
420 1367-2630/17/11/113013.
- 421 [54] W. Herreman, C. Nore, L. Cappanera, J.-L. Guermond, Tayler instability
422 in liquid metal columns and liquid metal batteries, *J. Fluid Mech.* 771
423 (2015) 79–114. doi:10.1017/jfm.2015.159.
- 424 [55] F. Stefani, V. Galindo, A. Giesecke, N. Weber, T. Weier, The Tayler in-
425 stability at low magnetic Prandtl numbers: Chiral symmetry breaking and
426 synchronizable helicity oscillations, *Magnetohydrodynamics* 53 (1) (2017)
427 169–178.
- 428 [56] T. Weier, A. Bund, W. El-Mofid, G. M. Horstmann, C.-C. Lalau, S. Land-
429 graf, M. Nimtz, M. Starace, F. Stefani, N. Weber, Liquid metal batteries
430 - materials selection and fluid dynamics, *IOP Conf. Ser. Mater. Sci. Eng.*
431 228 (012013).
- 432 [57] Y. Shen, O. Zikanov, Thermal convection in a liquid metal battery,
433 *Theor. Comput. Fluid Dyn.* 30 (4) (2016) 275–294. doi:10.1007/
434 s00162-015-0378-1.

- 435 [58] T. Köllner, T. Boeck, J. Schumacher, Thermal Rayleigh-Marangoni convec-
436 tion in a three-layer liquid-metal-battery model, *Phys. Rev. E* 95 (053114).
437 doi:10.1103/PhysRevE.95.053114.
- 438 [59] O. Zikanov, Metal pad instabilities in liquid metal batteries, *Phys. Rev. E*
439 92 (063021).
- 440 [60] N. Weber, P. Beckstein, V. Galindo, W. Herreman, C. Nore, F. Stefani,
441 T. Weier, Metal pad roll instability in liquid metal batteries, *Magnetohy-*
442 *drodynamics* 53 (1) (2017) 129–140.
- 443 [61] N. Weber, P. Beckstein, W. Herreman, G. M. Horstmann, C. Nore, F. Ste-
444 fani, T. Weier, Sloshing instability and electrolyte layer rupture in liq-
445 uid metal batteries, *Phys. Fluids* 29 (5) (2017) 054101. doi:10.1063/1.
446 4982900.
- 447 [62] V. Bojarevics, A. Tucs, MHD of Large Scale Liquid Metal Batteries, in:
448 A. P. Ratvik (Ed.), *Light Metals 2017*, Springer International Publishing,
449 Cham, 2017, pp. 687–692.
- 450 [63] G. M. Horstmann, N. Weber, T. Weier, Coupling and stability of interfacial
451 waves in liquid metal batteries, *ArXiv Prepr. ArXiv170802159*.
- 452 [64] D. H. Kelley, D. R. Sadoway, Mixing in a liquid metal electrode, *Phys.*
453 *Fluids* 26 (5) (2014) 057102. doi:10.1063/1.4875815.
- 454 [65] V. Sobolev, Thermophysical properties of lead and lead–bismuth eutectic,
455 *J. Nucl. Mater.* 362 (2-3) (2007) 235–247. doi:10.1016/j.jnucmat.2007.
456 01.144.
- 457 [66] V. Sobolev, *Database of Thermophysical Properties of Liquid Metal*
458 *Coolants for GEN-IV, SCK CEN*, 2010.
- 459 [67] N. E. Agency, *Handbook on Lead-bismuth Eutectic Alloy and Lead Prop-*
460 *erties, Materials Compatibility, Thermalhydraulics and Technologies*, Tech.
461 *Rep. 7268*, Nuclear Energy Agency (2015).

- 462 [68] P. Personnettaz, Assessment of thermal phenomena in Li||Bi liquid metal
463 batteries through analytical and numerical models, master thesis, Politec-
464 nico di Torino (2017).
- 465 [69] W. Wang, K. Wang, Simulation of thermal properties of the liquid metal
466 batteries, in: 6th International Conference on Power Electronics Systems
467 and Applications (PESA), IEEE, 2015, pp. 1–11.
- 468 [70] N. Weber, Modellierung von Tayler-Instabilität und Elektrowirbel-
469 strömungen in Flüssigmetallbatterien, Ph.D. thesis, Technische Universität
470 Dresden (2016).
- 471 [71] H. G. Weller, G. Tabor, H. Jasak, C. Fureby, A tensorial approach to com-
472 putational continuum mechanics using object-oriented techniques, *Comput.*
473 *Phys.* 12 (6) (1998) 620–631.
- 474 [72] N. Weber, P. Beckstein, V. Galindo, M. Starace, T. Weier, Electro-vortex
475 flow simulation using coupled meshes, *ArXiv Prepr. ArXiv170706546*.
- 476 [73] A. Oberbeck, Über die Wärmeleitung der Flüssigkeiten bei der
477 Berücksichtigung der Strömungen infolge von Temperaturdifferenzen, *Ann.*
478 *Phys. Chem.* 7 (271).
- 479 [74] D. D. Gray, A. Giorgini, The validity of the Boussinesq approximation for
480 liquids and gases, *Int. J. Heat Mass Transf.* 19 (5) (1976) 545–551.
- 481 [75] S. B. Dement’ev, O. M. Skopis, E. V. Sherbinin, Intensification of the mix-
482 ing process in direct-current electric arc furnaces, *Magnetohydrodynamics*
483 28 (1) (1992) 89–92.
- 484 [76] I. Kolesnichenko, S. Khripchenko, D. Buchenau, G. Gerbeth, Electro-vortex
485 flows in a square layer of liquid metal, *Magnetohydrodynamics* 41 (2005)
486 39–51.
- 487 [77] R. A. Woods, D. R. Milner, Motion in the weld pool in arc welding, *Weld.*
488 *J.* 50 (1971) 163–173.

- 489 [78] I. E. Butsenieks, D. E. Peterson, V. I. Sharamkin, E. V. Sherbinin, Mag-
490 netohydrodynamic fluid flows in a closed space with a nonuniform electric
491 current, *Magn. Gidrodin.* 1 (1976) 92–97.
- 492 [79] V. V. Boyarevich, V. I. Sharamkin, MHD flows due to current spreading in
493 an axisymmetric layer of finite thickness, *Magn. Gidrodin.* 2 (1977) 55–60.
- 494 [80] V. G. Zhilin, Y. P. Ivochkin, A. A. Oksman, G. R. Lurin'sh, A. I.
495 Chaikovskii, A. Y. Chudnovskii, E. V. Shcherbinin, An experimental in-
496 vestigation of the velocity field in an axisymmetric electrovortical flow in a
497 cylindrical container, *Magn. Gidrodin.* 3 (1986) 110–116.
- 498 [81] D. Rübiger, Y. Zhang, V. Galindo, S. Franke, B. Willers, S. Eckert, The
499 relevance of melt convection to grain refinement in Al–Si alloys solidified
500 under the impact of electric currents, *Acta Mater.* 79 (2014) 327–338. doi :
501 10.1016/j.actamat.2014.07.037.
- 502 [82] D. R. Atthey, A mathematical model for fluid flow in a weld pool at high
503 currents, *J. Fluid Mech.* 98 (4) (1980) 787–801.
- 504 [83] P. A. Davidson, S. C. Flood, Natural convection in an aluminum ingot: A
505 mathematical model, *Metall. Mater. Trans. B* 25 (2) (1994) 293–302.
- 506 [84] P. A. Davidson, D. Kinnear, R. J. Lingwood, D. J. Short, X. He, The role
507 of Ekman pumping and the dominance of swirl in confined flows driven by
508 Lorentz forces, *Eur. J. Mech. - BFluids* 18 (1999) 693–711.
- 509 [85] P. A. Davidson, Overcoming instabilities in aluminium reduction cells: A
510 route to cheaper aluminium, *Mater. Sci. Technol.* 16 (5) (2000) 475–479.
- 511 [86] A. Kharicha, W. Schützenhöfer, A. Ludwig, R. Tanzer, M. Wu, On the
512 importance of electric currents flowing directly into the mould during an
513 ESR process, *Steel Res. Int.* 79 (8) (2008) 632–636.
- 514 [87] V. Shatrov, G. Gerbeth, Stability of the electrically induced flow between
515 two hemispherical electrodes, *Magnetohydrodynamics* 48 (3).

- 516 [88] O. V. Kazak, A. N. Semko, Numerical modeling of electro-vortical flows in
517 a confined volume, *J. Eng. Phys. Thermophys.* 85 (2012) 1167–1178.
- 518 [89] A. Kharicha, I. Teplyakov, Y. Ivochkin, M. Wu, A. Ludwig, A. Gu-
519 seva, Experimental and numerical analysis of free surface deformation in
520 an electrically driven flow, *Exp. Therm. Fluid Sci.* 62 (2015) 192–201.
521 doi:10.1016/j.expthermflusci.2014.11.014.
- 522 [90] O. Kazak, A. Semko, Modelling vortex fields in metal smelting furnaces,
523 *Int. J. Multiphysics* 4 (4).
- 524 [91] O. V. Kazak, A. N. Semko, Electro-vortex motion of a melt in DC furnaces
525 with a bottom electrode, *J. Eng. Phys. Thermophys.* 84 (1) (2011) 223–231.
- 526 [92] O. Kazak, Modeling of Vortex Flows in Direct Current (DC) Electric Arc
527 Furnace with Different Bottom Electrode Positions, *Metall. Mater. Trans.*
528 *B* 44 (5) (2013) 1243–1250. doi:10.1007/s11663-013-9899-4.
- 529 [93] O. Semko, Y. Ivochkin, I. Teplyakov, K. O., Electro vortex flows in hemi-
530 sphere volume with different bottom electrode positions, in: 9th PAMIR
531 International Conference, Fundamental and Applied MHD, 2014.
- 532 [94] A. Beltrán, MHD natural convection flow in a liquid metal electrode, *Appl.*
533 *Therm. Eng.* 114 (2016) 1203–1212. doi:10.1016/j.applthermaleng.
534 2016.09.006.
- 535 [95] V. Bojarevičs, E. V. Shcherbinin, Azimuthal rotation in the axisymmetric
536 meridional flow due to an electric-current source, *J. Fluid Mech.* 126 (1983)
537 413–430.
- 538 [96] P. Davidson, X. He, A. Lowe, Flow transitions in vacuum arc remelt-
539 ing, *Mater. Sci. Technol.* 16 (6) (2000) 699–711. doi:10.1179/
540 026708300101508306.